Contents lists available at AccScience Publishing
Nonlinear Science and Control Engineering (NSCE)
Vol. 1, No. 2 (2025)
https://accscience.com/journal/nsce

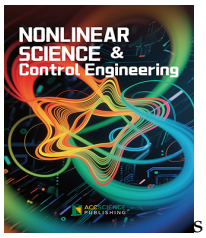

Complex neuronal dynamics under memristive electromagnetic radiation: Modeling and digital signal processing implementation

Fan Shi[1], Xianying Xu[1*], Xiaodong Liu[2*], Yinghong Cao[1], Suo Gao[1], and Jun Mou[1]

[1]*School of Information Science and Engineering, Dalian Polytechnic University, Dalian, Liaoning, China*
[2]*School of Innovation and Entrepreneurship, Dalian Polytechnic University, Dalian, Liaoning, China*

Article History:
Received: September 29, 2025
Revised: October 14, 2025
Accepted: October 20, 2025
Published online: November 17, 2025

ABSTRACT

The development of artificial neural networks requires breaking through the limitations of traditional models to establish architectures that more closely resemble the real characteristics of biological neural systems. This paper proposes a novel locally active discrete memristor model and incorporates it into a Hopfield neural network to investigate the influence of electromagnetic radiation (EMR) on neuronal dynamics. By employing nonlinear analysis methods, the complex dynamical characteristics of the system are systematically examined, including bifurcation diagrams, Lyapunov exponent spectra, phase trajectories, and firing patterns. The results demonstrate that the system exhibits diverse nonlinear behaviors, including multistability, state transitions, and attractor offset control, under different parameter conditions. Moreover, by adjusting the memristor parameter, flexible regulation of the dynamical states can be achieved. To further validate the feasibility of the proposed model, a digital signal processing-based hardware implementation is designed and tested. The findings not only simulate the intricate dynamical responses of neurons under EMR exposure but also reveal rich nonlinear phenomena, providing potential applications in medical diagnosis and secure image encryption.

Keywords: Attractor control; Hyperchaos; Memristor; Multistability; Neural network

1. Introduction

The human brain is a highly complex neural network system composed of hundreds of billions of neurons interconnected by synapses, enabling humans to think, perceive, and act.[1,2] Each neuron transmits, receives, and processes information through numerous synapses, exhibiting highly nonlinear behaviors across micro to macroscales.[2,3] To gain a deeper understanding of the structure and function of biological neural networks (BNNs) and to simulate their operational mechanisms, extensive research efforts have been devoted, leading to

***Corresponding authors**:
Xianying Xu (xuxiany@dlpu.edu.cn).
Xiaodong Liu (liuxiaod@dlpu.edu.cn).

Citation:
Shi F, Xu X, Liu X, Cao Y, Gao S, Mou J. Complex neuronal dynamics under memristive electromagnetic radiation: Modeling and digital signal processing implementation. *Nonlinear Sci Cont Eng.* 2025;1(2):025400013. doi: 10.36922/NSCE025400013

the development of artificial neural networks (ANNs).[4] ANNs possess information-processing capabilities similar to those of BNNs, providing important insights into neural network operation and finding broad applications in pattern recognition, intelligent computing, machine vision, and predictive control.[5] The construction of neuron models is a crucial step in understanding biological neural systems and advancing artificial intelligence.[6] Since the introduction of the Hopfield neural network (HNN) in 1982, research on ANNs has accelerated rapidly.[4] Classical neuron models, such as the Hodgkin–Huxley, Hindmarsh–Rose, and FitzHugh–Nagumo models, provide theoretical foundations for simulating neuronal electrophysiological characteristics.[7] In recent years, the development of electronic devices, such as memristors, has further improved the construction of artificial neuron models, offering important guidance for the design of ANNs.[8] Meanwhile, electromagnetic radiation (EMR), as an external environmental factor, has attracted increasing attention for its potential impact on neuronal dynamics.[9] Studies have shown that EMR can alter information processing by perturbing neuronal electrophysiological properties and synaptic plasticity, potentially affecting cognitive functions and behavior.[10] Ma et al.[11] observed that introducing EMR into neuron models via memristors can generate hidden multiscroll attractors and initially enhanced behaviors. Zhang et al.[12] incorporated two distinct memristors into an HNN—one serving as a memristive synapse and the other as an EMR—to enhance chaotic complexity.

Chaos theory has been widely applied in neuroscience to explain the complex dynamic behaviors observed in electroencephalographic activity.[13] The brain is a highly complex system, where minor differences in initial conditions (ICs) can lead to significant variations, a characteristic consistent with typical chaotic systems.[14] Nonlinear analyses have revealed that brain activity exhibits positive Lyapunov exponents (LEs), providing strong evidence for the presence of chaos.[15] The integration of dynamical systems theory with neuroscience has given rise to the emerging field of neurodynamics, which employs nonlinear dynamical methods to investigate the temporal evolution of biological neural systems and their chaotic properties, including firing patterns.[16,17] Moreover, chaos theory has been incorporated into ANNs to simulate the dynamic behaviors of the brain and its remarkable capabilities for efficient information processing and storage, thereby facilitating the development of computational models that exhibit brain-like behaviors.[18,19] In this context, Li et al.[20] proposed an HNN with dual-sequence interconnections, enabling chaotic attractors to switch between different planar positions depending on the initial state. He et al.[21] developed a model combining asymmetric neural networks with fractional-order differences, demonstrating the existence of coexisting state variables under specific ICs, thereby revealing the emergence of multilayer attractors. Shi et al.[22] applied a novel nonvolatile second-order memristor to a resistor, inductor, and capacitor neuron model to simulate synaptic connections and electromagnetic interactions, uncovering rich bifurcation behaviors and extreme multistability.

The memristor is a two-terminal device with a unique memory function, whose conductance varies with the current passing through it.[23,24] This property provides a distinct advantage in modeling synaptic plasticity observed during neuronal signal transmission.[25,26] In memristive neuron models, the memristor can replace potassium and sodium ion channels at synapses, enabling a more accurate representation of fundamental neuronal functions.[27] Moreover, the definition of the memristor reveals a unique relationship between magnetic flux and electric charge.[28] As the basic unit of biological neural systems, neurons also exhibit functions and structures closely related to electromagnetic interactions.[29] External EMR affecting neurons can be interpreted as acting through the magnetic flux across the membrane, which is tightly coupled with charge movement and further modulates neuronal firing behavior and information transmission.[30] Therefore, memristive neuron models not only effectively simulate dynamic changes in synaptic conductance but also capture the influence of external electromagnetic stimuli on neuronal dynamics, providing a powerful tool for a deeper understanding of complex neuronal information processing mechanisms.[31,32] Building on the inductive currents of memristive synapses, Bao et al.[33] proposed a memristor-enhanced Morris–Lecar model, revealing various period-doubling bifurcations, as well as rich periodic and chaotic firing behaviors. Shen et al.[34] introduced a composite hyperbolic tangent cubic nonlinear memristor, featuring both nonvolatile and locally active characteristics. When applied to neuron models, this memristor exhibited diverse brain-like firing patterns, offering new theoretical tools and methods for the study of neuronal dynamics.

Based on the aforementioned background, this study proposes a neuron model that accounts for the effects of EMR. The model employs discrete memristors to simulate and quantify the mechanisms by which EMR influences neuronal activity. Unlike previous studies, this work constructs a discrete neuron model grounded in physiological experiments, enabling a more precise representation of the electrophysiological characteristics of neurons. The advantage of this approach lies not only in its ability to more realistically simulate neuronal dynamic behavior but also in providing a more reliable theoretical and experimental basis for investigating the effects of EMR on the complex nonlinear dynamics of neurons.

The remainder of this paper is organized as follows. Section 2 introduces the proposed model and presents a stability analysis. Section 3 conducts numerical simulations to investigate dynamic behavior, multistability, and attractor offset control of the model. Section 4 describes the implementation of the model on a digital signal processing (DSP) platform. Finally, Section 5 concludes the paper.

2. Model introduction and stability analysis

This section proposes utilizing discrete memristors to simulate EMR behavior and presents the constructed neuron model. Furthermore, the equilibrium points and stability of the model are analyzed, laying the foundation for subsequent theoretical investigations.

2.1. Locally active memristor with threshold

Memristors exhibit synaptic plasticity and hold significant applications in constructing ANNs. Additionally, memristors can characterize the relationship between magnetic flux and charge, enabling their use in simulating EMR in neuronal models and thereby investigating the effects of EMR on neurons. In this work, a discrete

memristor with locally active characteristics is proposed, with adjustable threshold capability. Discretization is performed using forward Eulerian differences.[35] The memristor model can be described as Equation (1).

$$\begin{cases} v_n = k\tanh(q_n)i_n \\ q_{n+1} = a([q_n+1]+[q_n-1]+q_n)+b+i_n \end{cases} \quad (1)$$

Where v_n, i_n, and q_n are the voltage across the memristor, the current flowing through the memristor, and the magnetic flux, respectively. The $tanh$ function with upper and lower thresholds, similar to the threshold change of biological synaptic weights. Parameter k is the amplitude adjustment parameter for the threshold-type locally active memristor (LAM), while a and b are internal parameters of the memristor.

To verify whether the model meets the definition of a memristor, the pinched hysteresis loop (PHL) of the model is used for determination. When a sinusoidal voltage signal, $i_n = V_m\sin(2\pi fn)$, is applied to the model, a figure-of-eight curve is presented in the v_n–i_n plane. When parameters a = 1, b = 1, and k = 10 are set, the PHL is exhibited by adjusting the amplitude and frequency of the input sin function, as shown in Figure 1A and 1B. At a fixed frequency f = 1, the area surrounded by the PHL increases as the amplitude of the input signal increases. When the amplitude V is set to 1 and the frequency is varied, the PHL shrinks as the frequency increases. When the frequency increases to a certain level, the memristor behaves as a linear resistor. Through numerical simulation, it can be clearly observed that this model meets the definition of a memristor. To further demonstrate the applicability of the model, with fixed amplitude V = 1 and frequency f = 1, varying the internal parameters a and b of the system resulted in the PHL of the memristor consistently exhibiting an inverted "8" shape, as shown in Figure 1C and 1D, respectively. This confirms the strong robustness of the model.

Nonvolatility is one of the most important characteristics of memristors, enabling their application in constructing large-scale ANNs. The memristor proposed in this work also exhibits nonvolatility. To demonstrate this property, setting i_n = 0 transforms the state equation into Equation (2).

$$q_{n+1}-q_n = a\,\mathrm{sgn}(q_n+1)+a\,\mathrm{sgn}(q_n-1)+(a-1)q_n+b \quad (2)$$

The power-off plot (POP) of the memristor is shown in Figure 2A. It clearly reveals three negative slope intersections with the x-axis in the POP. Based on this, the memristor is a nonvolatile memristor.

Local active character is the origin of complexity, and memristors exhibiting this property often display complex dynamic behavior. To investigate the local active character of this model, it can be assessed through the direct current voltage–current (DC $V-I$) curve of the memristor. Setting $q_{n+1}-q_n = 0$ and $i_n = I$, it can be derived into Equation (3).

$$\begin{cases} I = -a\,\mathrm{sgn}(q_n+1)-a\,\mathrm{sgn}(q_n-1)+(1-a)q_n-b \\ V = k\tanh(q_n)I = k\tanh(q_n)(-a\,[q_n+1]-a\,\mathrm{sgn}\,[q_n-1]+[1-a]\,q_n-b) \end{cases} \quad (3)$$

When a negative slope region appears in the DC $V-I$ curve, the memristor exhibits LAM behavior. By setting q_n to vary within the range $(-1, 1)$, a negative slope region can be observed in Figure 2B. Therefore, this memristor is classified as a LAM.

2.2. Neuron model

Neuroscientists have had mathematical models of neurons designed by studying the structure and functioning of biological nervous systems. To better estimate the information interaction mechanisms of neurons, HNNs are widely employed. Previous studies have demonstrated that HNNs are particularly suitable for simulating complex dynamic behaviors in the brain. This work employs a two-dimensional discrete model of dual-neuron HNN featuring both self-connections and coupled connections. Its mathematical model is shown in Equation (4).

$$\begin{cases} x_{n+1} = \mu x_n + w_{11}\tanh(x_n) + w_{12}\tanh(y_n) \\ y_{n+1} = \mu y_n + w_{21}\tanh(x_n) + w_{22}\tanh(y_n) \end{cases} \quad (4)$$

Here, x_{n+1} and y_{n+1} represent the membrane potentials of two Hopfield neurons, while the parameter μ denotes the internal decay variable of the neuron. The parameters w_{11}, w_{12}, w_{21}, and w_{22} correspond to the synaptic connection weights, and the tanh function is selected as the activation function for the system. Introducing memristors into the neuronal model exposes neurons to the effects of EMR, resulting in the dynamical Equation (5).

$$\begin{cases} x_{n+1} = \mu x_n + w_{11}\tanh(x_n) + w_{12}\tanh(y_n) + k\tanh(z_n)x_n \\ y_{n+1} = \mu y_n + w_{21}\tanh(x_n) + w_{22}\tanh(y_n) \\ z_{n+1} = a((z_n+1)+(z_n-1)+z_n)+b+x_n \end{cases} \quad (5)$$

The x_{n+1}, y_{n+1}, and z_{n+1} represent the state variables of the model, while k denotes the intensity of EMR. The neural model under EMR is illustrated in Figure 3.

With fixed synaptic connection weights, the state equations of the system can be expressed as Equation (6).

$$\begin{cases} x_{n+1} = \mu x_n + 3\tanh(x_n) + 10\tanh(y_n) + k\tanh(z_n)x_n \\ y_{n+1} = \mu y_n - 2\tanh(x_n) + 2\tanh(y_n) \\ z_{n+1} = a(\mathrm{sgn}(z_n+1)+\mathrm{sgn}(z_n-1)+z_n)+b+x_n \end{cases} \quad (6)$$

Setting the remaining parameters to μ = 0.8, $k = 1$, $a = 0.9$, $b = -2$, and ICs (0, 0.1, 0), the LEs of the system are calculated as LE1 = 0.3166, LE2 = -0.1053, and LE3 = -1.4742. At this time, the system exhibits positive LEs, indicating that it is in a chaotic state. To further verify its dynamic properties, the LE dimension, D_L, of the system is calculated as D_L = 2.1433. Since D_L satisfies $2 < D_L < 3$, the attractor is identified as a chaotic attractor embedded in three-dimensional phase space. The fractional value of the Lyapunov dimension indicates that the attractor possesses a fractal geometry, exhibiting chaotic behavior with trajectories that partially fill the three-dimensional space rather than occupying it completely. The corresponding chaotic attractor is shown in Figure 4.

2.3. Equilibrium analysis and stability

Equilibrium point analysis is an important method for identifying equilibrium points to analyze the stability of chaotic systems. Let both sides of the equation be equal, as shown in Equation (7).

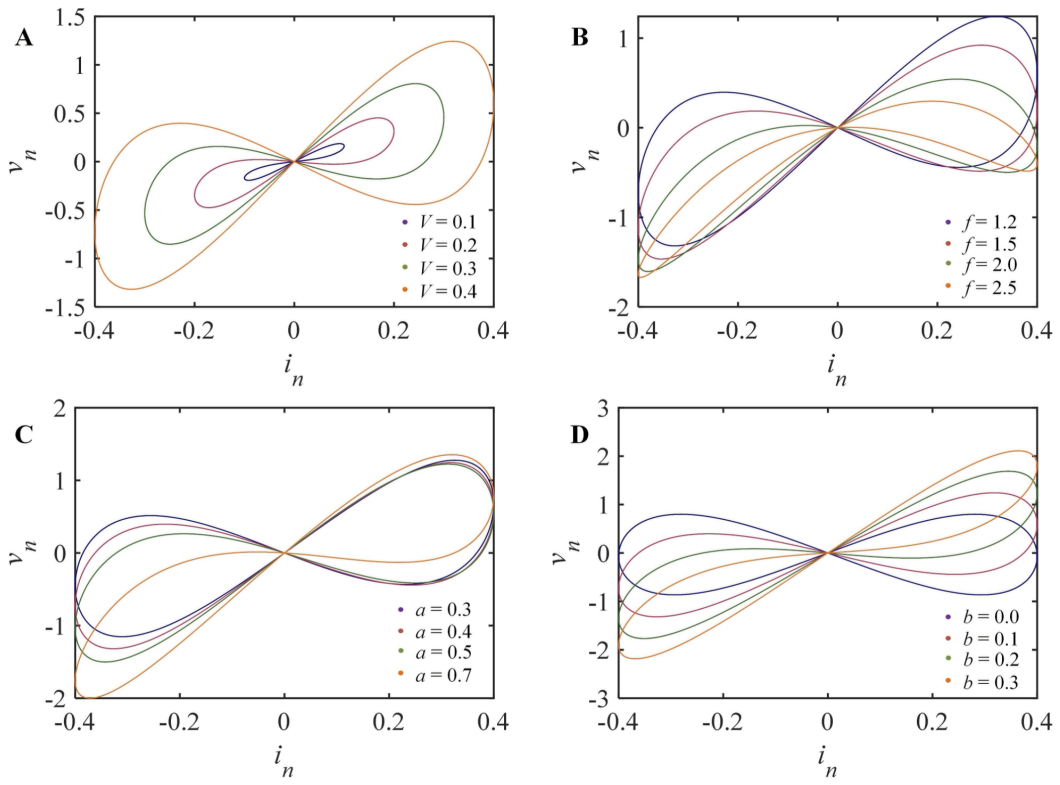

Figure 1. The pinched hysteresis loop of the memristor. (A) V = 0.1, 0.2, 0.3, and 0.4; f = 1. (B) f = 1.2, 1.5, 2.0, and 2.5, V = 0.5. (C) a = 0.3, 0.4, 0.5, and 0.7; b = 0.1. (D) b = 0.0, 0.1, 0.2, and 0.3; a = 0.3.

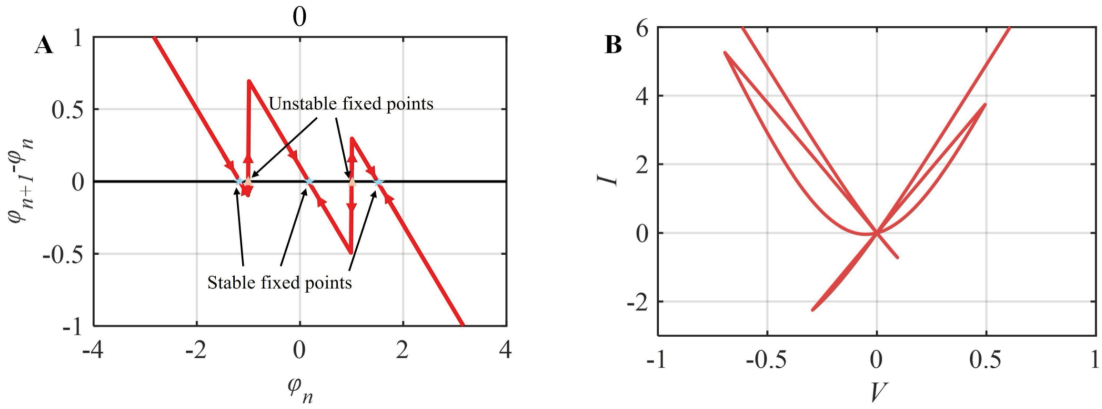

Figure 2. Power-off plot and direct current voltage–current plot. (A) $\phi = (-4, 4)$. (B) $V = (-1, 1)$.

$$\begin{cases} x_n^* = \mu x_n^* + w_{11}\tanh(x_n^*) + w_{12}\tanh(y_n^*) + k\tanh(z_n^*)x_n^* \\ y_n^* = \mu y_n^* + w_{21}\tanh(x_n^*) + w_{22}\tanh(y_n^*) \\ z_n^* = a(\mathrm{sgn}\,[z_n^* + 1] + \mathrm{sgn}\,[z_n^* - 1] + z_n^*) + b + x_n^* \end{cases} \tag{7}$$

By solving Equation (7), the immobile points of the model $(x_n^* = 0, y_n^* = 0, z_n^* = z)$ can be easily solved, where the values of z are determined by the range of z and the parameter values of a and b Equation (8).

$$z_n^* = \begin{cases} \frac{b+2a}{1-a}, & z_n^* < -1 \\ \frac{b}{1-a}, & -1 < z_n^* < 1 \\ \frac{b+2a}{1-a}, & z_n^* > 1 \end{cases} \tag{8}$$

After obtaining the equilibrium point, it is carried into the Jacobian matrix of Equation (7) to further derive the characteristic equation for stability analysis. The Jacobian matrix of the model is shown in Equation (9).

$$J = \begin{pmatrix} \mu + w_{11} + k\tanh(z) & w_{12} & 0 \\ w_{21} & \mu + w_{22} & 0 \\ 1 & 0 & a \end{pmatrix} \tag{9}$$

Thus, the characteristic equation of the system can be written as Equation (10).

$$\begin{aligned} P(\lambda) = (a - \lambda)([\mu + w_{11} + k\tanh z - \lambda] \\ [\mu + w_{22} - \lambda] - w_{12}w_{21}) \end{aligned} \tag{10}$$

Based on the characteristic equation, the eigenvalues can be solved, where $\lambda_1 = a$, while λ_2, and λ_3 are the roots of a quadratic equation related to the parameters. When λ_2 and λ_3 are disregarded and the absolute value of a is

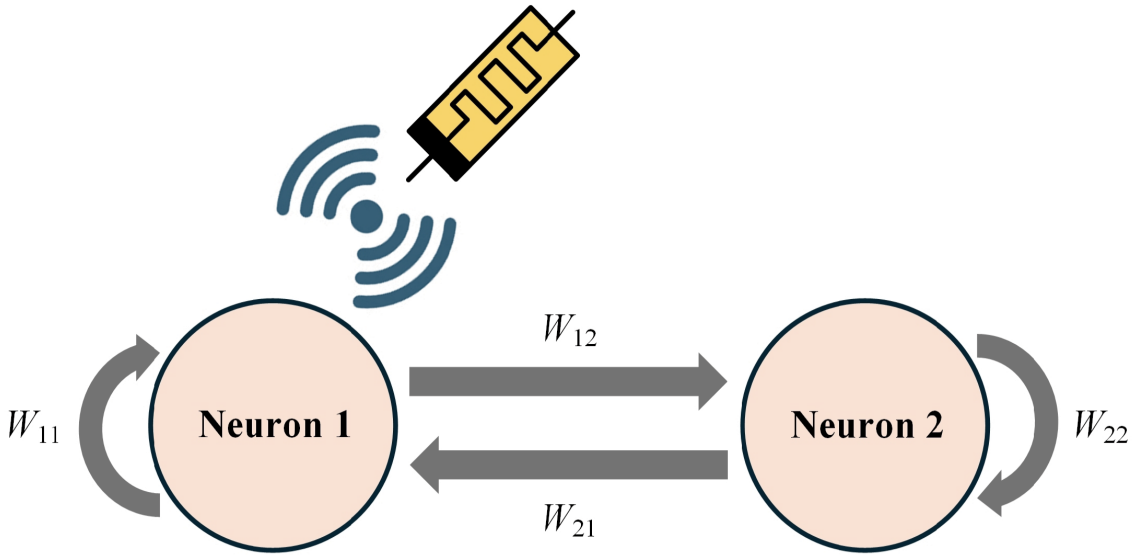

Figure 3. Topological model under electromagnetic radiation

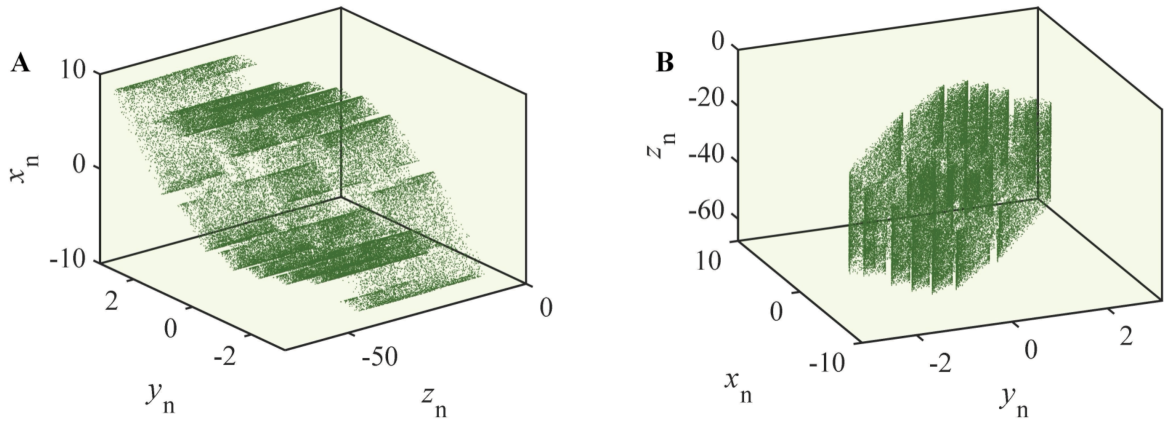

Figure 4. Three-dimensional chaotic attractor. (A) $z_n - y_n - x_n$ plane. (B) $y_n - x_n - z_n$ plane.

less than 1, the system is in a stable state. This quadratic equation can be expressed as Equation (11).

$$\lambda^2 - (\mu + w_{11} + k\tanh z + \mu + w_{22})\lambda + (\mu + w_{11} + k\tanh z)(\mu + w_{22}) - w_{12}w_{21} = 0 \quad (11)$$

From Equation (11), it is evident that the stability of the system depends on the values of multiple parameters. Therefore, by fixing the parameters $w_{11} = -3, w_{12} = 10, w_{21} = -2, w_{22} = 2, \mu = 0.8, a = 0.9, b = -2$, the curves of the characteristic values of the system as a function of the coupling strength k can be plotted, as shown in Figure 5. For discrete models, the system is asymptotically stable when all eigenvalues are less than 1. It can be observed that as memristor parameters vary, unstable regions may emerge, potentially exhibiting complex dynamical behavior.

3. Dynamical analyses

Numerical simulation methods enable the quantitative analysis of complex dynamical behaviors within systems. In this section, various tools, such as bifurcation diagrams, LE spectra, and firing diagrams, are used to uncover the complex dynamical behaviors present in the system, including multiple bifurcations, multistability, state transitions, and multi-state offsets.

3.1. Bifurcation behavior in relation to parameters

Analysis of the equilibrium points and stability reveals that parameters have a significant influence on the state of the system, and different parameters can cause the system to exhibit different dynamic behaviors. Based on this, it is necessary to perform a numerical analysis of the dynamical state of the system using a bifurcation diagram, as shown in Figure 6. When parameters are set as $a = 0.95, b = -2, k = 1$, and IC = (0, 0.1, 0), the bifurcation diagram and LEs for the neuron parameter μ in the range $(-0.3, 0.9)$ are shown in Figure 6A and 6D, respectively. The model initiated from a chaotic state. As μ increased to 0.1, the system state abruptly transitioned to a periodic state, resulting in the maximum LE becoming negative. The system then entered a stable periodic state until approximately μ = 0.4, when it began transitioning into an unstable orbit. From this point until 0.9, the system remained in a chaotic state. This process also included numerous periodic windows, demonstrating the system's exceptionally rich dynamical behavior and highlighting the significant influence of the neuron parameter μ on system stability. To further

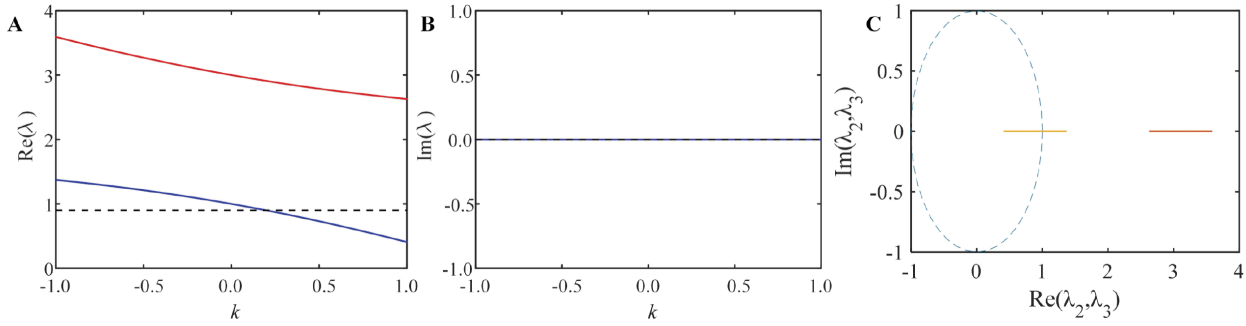

Figure 5. Eigenvalue trajectory plots for parameter variation. (A) Variation of eigenvalue real domain with k. (B) Variation of eigenvalue imaginary domain with k. (C) Variation of eigenvalue with k.

illustrate the effects of varying EMR intensities on neuronal dynamics, bifurcation diagrams and LEs with radiation strength k = (0, 1.5) are shown in Figure 6B and 6E, respectively. The bifurcation diagram reveals significant changes in the shape of the attractor with varying EMR strength. As k increased, the attractor exhibited contraction. When k reached 1.2, the system state transitioned from chaotic to periodic. Subsequently, after multiple state transitions, the system finally stabilized in a chaotic state at 1.42 through bifurcation. Memristor parameters are often decisive for the dynamical state of neurons; when the memristor parameter a = (0, 1), the system underwent multiple chaotic and periodic state transitions. The system exhibited multiple bifurcation behaviors, transitioning into a chaotic state via double-period bifurcation at a = 0.4 and into a periodic state via tangent bifurcation at a = 0.7. Based on the above bifurcation analysis of neuron parameters, EMR strength, and memristor parameters, it is evident that the stability of the system depends on multiple parameters. This system exhibited extremely high parameter sensitivity, making it suitable for applications like chaotic image encryption.

To further illustrate the distinct dynamical states of the system, Figure 7 illustrates the attractors and firing patterns for the neuronal parameter μ. Under the parameter selection in Figure 7B, the system exhibits periodic behavior, while under other parameter selections, it demonstrates various chaotic characteristics. As shown in Figure 7E–H, the firing patterns corresponding to the z-sequences of the attractors reveal that the firing patterns in chaotic states exhibit significantly more random characteristics compared to the periodic state. Figure 8 depicts attractors of the system under different EMR strengths. Here, two distinct chaotic attractors were selected for k = 0.5 and k = 1, along with a periodic attractor for k = 1.2. The corresponding firing patterns are shown in Figure 8D, 8E, and 8F. In neurophysiology, the time interval between two consecutive action potentials of a neuron is referred to as the interspike interval (ISI). The ISI characteristics of a neural model directly influence the firing patterns of neurons. This study showed that changes in the coupling strength k affected the ISI, leading to critical transitions in neuronal dynamics. As k increased, the ISI histogram indicated that neuronal firing became stochastic, and the neuron transitioned from chaotic to periodic behavior, as shown in Figure 8. Figure 9 illustrates the attractors that are influenced by memristor parameters. Figure 9A and 9D depict chaotic attractors, while Figure 9B and 9C show periodic attractors. The attractors in Figure 9 reveal significant differences in topological structure, demonstrating that the introduction of memristors generates rich dynamics in the neural network.

3.2. State transition

When the fixed system parameters, μ = 0.2, a = 0.7, b = 1, and k = 0.9, the system undergoes a state transition on the timescale, evolving from a chaotic state to a stable periodic state. The attractors of this state transition are shown in Figure 10A, where purple represents the periodic attractor and orange represents the chaotic attractor. The corresponding firing patterns are illustrated in Figure 10B and 10C. The firing patterns reveal that periodic firing exhibits distinct regularity, whereas chaotic firing displays disordered behavior. To illustrate this temporal scale difference, Figure 10D presents the firing patterns of the z-sequence under this parameter. It is clearly observable that when n = 2,100, the system abruptly transitions from chaotic disordered firing patterns to regular periodic firing patterns. This state transition phenomenon originates from the inherent complexity and diversity within the system.

3.3. Multistability

Multistable chaotic dynamics is a crucial phenomenon in nonlinear dynamics, embodying the characteristic of complex systems where multiple stable states or attractors may coexist simultaneously, thereby revealing the richness and diversity of such models. When fixed parameters, $w_{11} = -2, w_{12} = 5, w_{22} = 2, a = 0.9, b = -3$, μ = 0.8, k = 1, and IC = (0.1, 0.1, z_0) were set, altering the ICs $z_0 = -1$ and $z_0 = 1$ revealed a phenomenon of symmetric coexisting attractors in the system. As the parameter, a, varied within the range (0, 1), the system exhibited coexisting bifurcation behavior, as shown in Figure 11A. The bifurcation diagram reveals that the system can achieve coexisting attractors by altering ICs, with these coexisting attractors symmetrically distributed about $z = 48$. To intuitively observe this unique dynamical phenomenon, three sets of coexisting attractors in different states are depicted in Figure 11B, 11C, and 11D. Figure 11B shows the coexisting attractors in the periodic state, where the periodic attractor appears as a point attractor. Figure 11C and 11D depict the coexisting attractors in the chaotic state, where the chaotic attractors manifest as singular attractors.

To further illustrate the impact of different ICs on system dynamics, the parameters were set as $w_{11} = -2, w_{12} = 5, w_{21} = 5, w_{22} = 2, a = 0.9, b = -3$, μ =

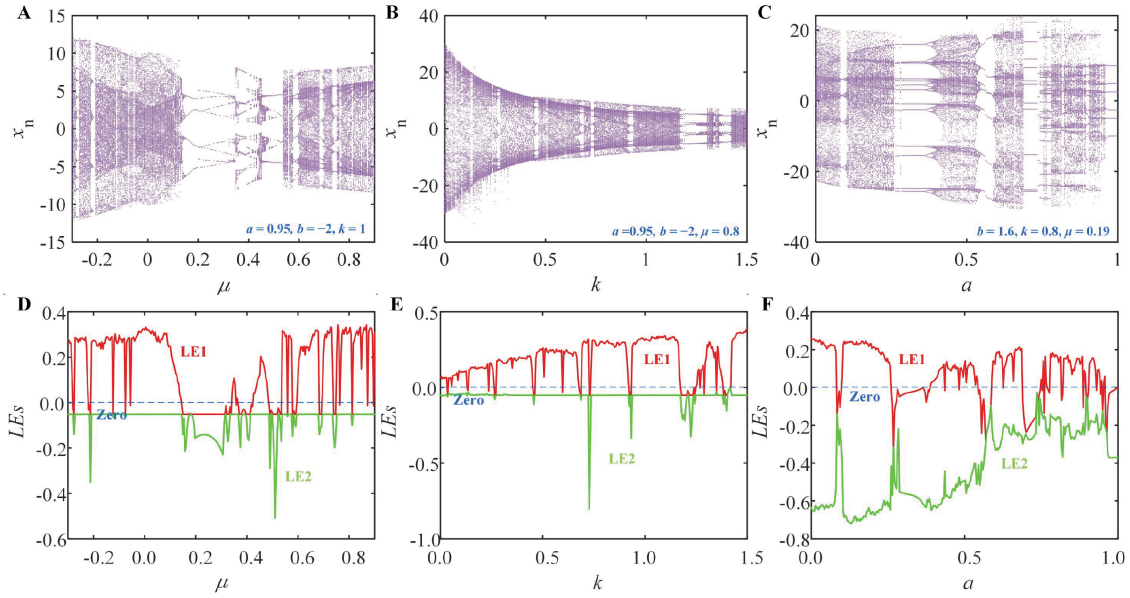

Figure 6. Bifurcation diagrams and Lyapunov exponents. (A) $a = 0.95, b = -2$ and $k = 1$, μ = (−0.3, −0.9). (B) a = 0.95, $b = -2$ and $\mu = 0.8, k$ = (0, 1.5). (C) b = 1.6, k = 0.8 and μ = 0.19, a = (0, 1). (D) a = 0.95, b = −2 and k = 1, μ = (−0.3, −0.9). (E) a = 0.95, b = −2 and μ = 0.8, k = (0, 1.5). (F) b = 1.6, k = 0.8 and μ = 0.19, a = (0, 1).

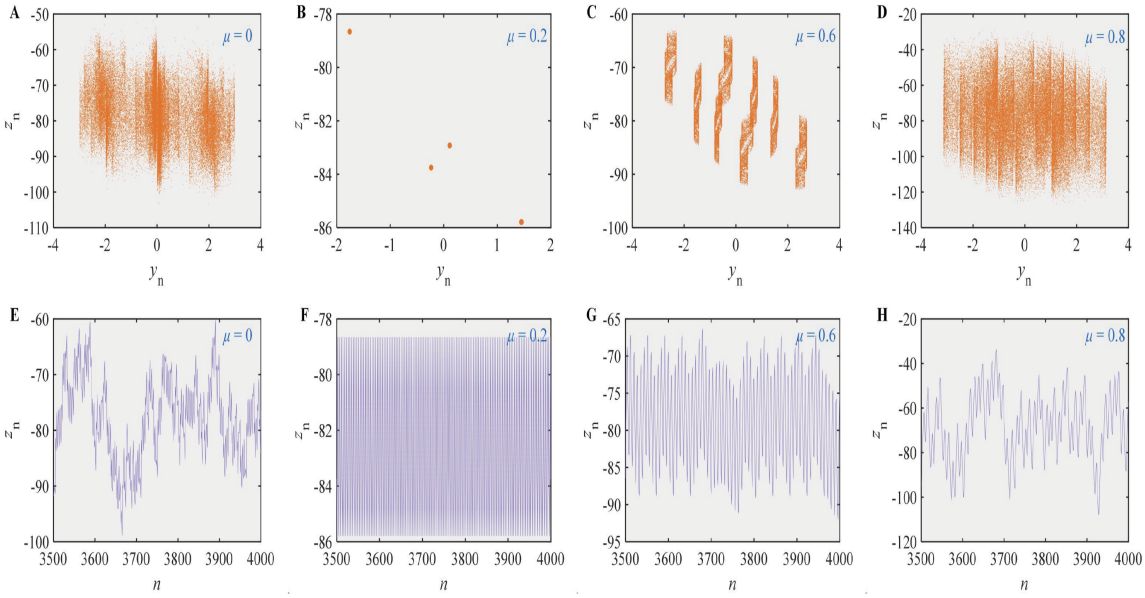

Figure 7. Attractors and firing plots of neuronal parameter μ. (A) Chaos attractor. (B) Period attractor. (C) Chaos attractor. (D) Chaos attractor. (E) Chaos firing. (F) Period firing. (G) Chaos firing. (H) Chaos firing.

(0,1), $k = 1$, and IC = (0.1, 0.1, 0). Figure 12 illustrates the attractor basins of the system under different ICs: x_n, y_n, and z_n. Different colors denote distinct dynamical states: CH represents chaotic states, MP denotes multiperiodic states, while P1, P2, P3, and P4 correspond to periodic states with periods 1, 2, 3, and 4, respectively. The multistability phenomenon revealed the high complexity of the phase structure at this parameter, resulting in minor differences in ICs to lead the system into distinct attractors.

3.4. Multistate offset behavior

In memristor-driven neuronal models, it is common to introduce external control equations to adjust the offset of attractors. However, controlling attractors via the internal state variables of the model has been rarely explored. In this work, both linear and nonlinear components of the neuronal model were considered. The unique nonlinear characteristics of the memristor endow the system with full offset controllability, enabling precise adjustment of attractor offsets.

To demonstrate the generality of this control approach, attractors under different system states were selected for offset regulation. The bifurcation diagrams corresponding to variations in the internal control parameter b are shown in Figure 13. Specifically, Figure 13A and 13D depict the LE spectra and bifurcation diagrams for periodic attractor offset control, Figure 13B and 13E for chaotic attractor offset control, and Figure 13C and 13F for hyperchaotic attractor offset control. It can be observed that under this

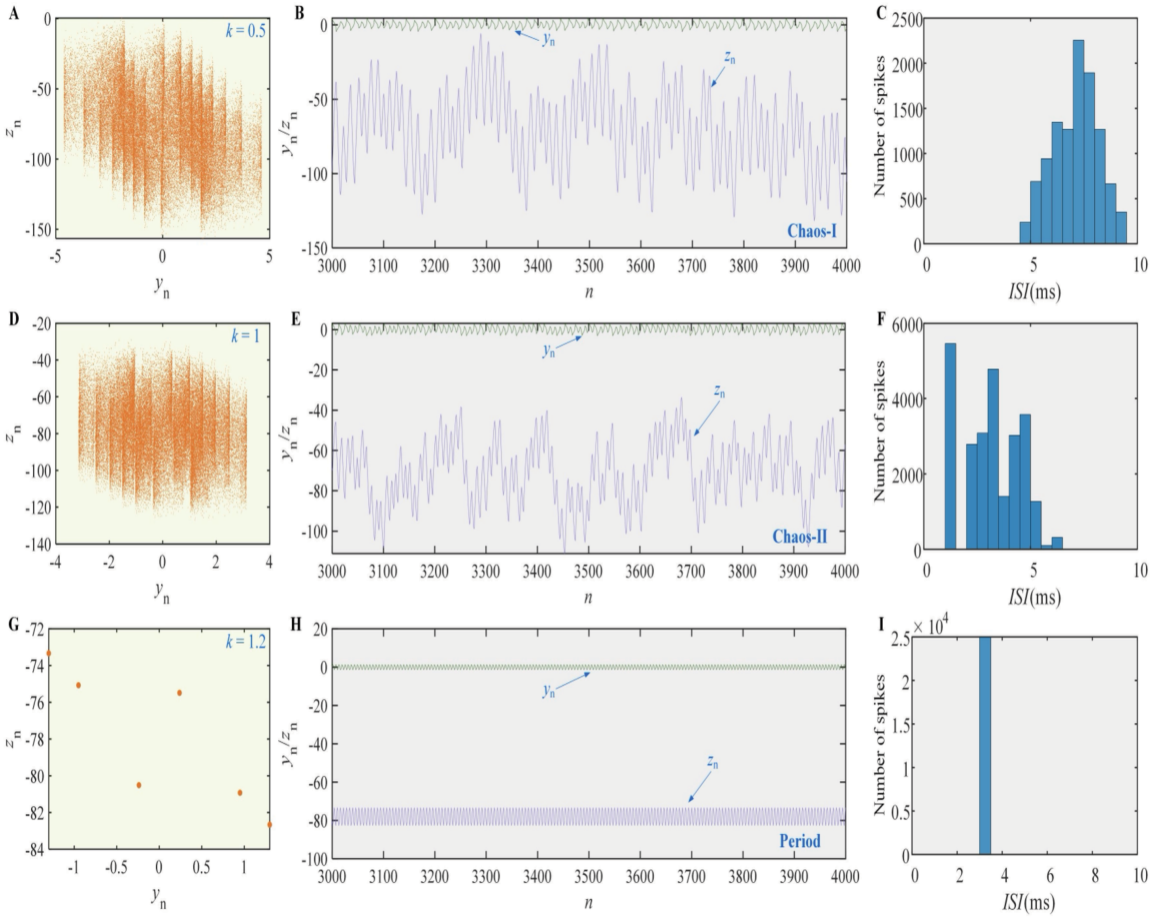

Figure 8. Attractors and firing plots of electromagnetic radiation strength k. (A) Chaos-I attractor. (B) Chaos-I firing. (C) ISI of chaos-I. (D) Chaos-II attractor. (E) Chaos-II firing. (F) ISI of chaos-II; (G) Period attractor. (H) Period firing; (i) ISI of period. Abbreviation: ISI: interspike interval.

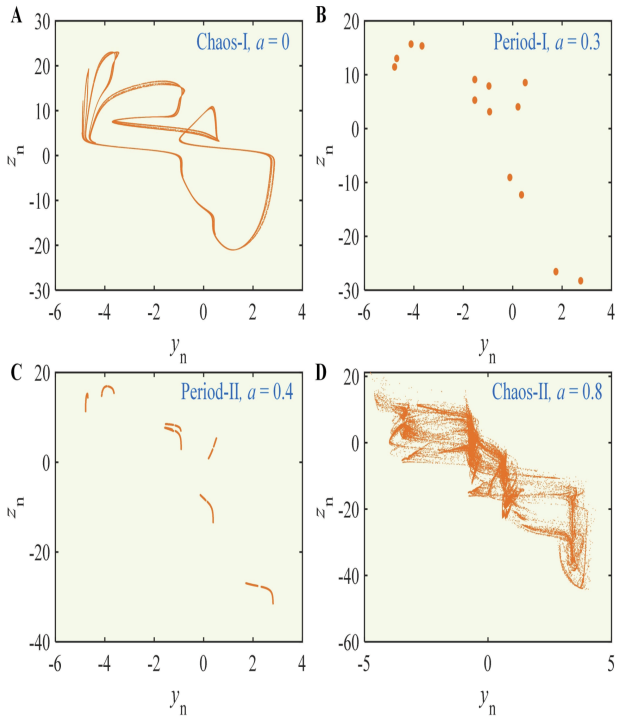

Figure 9. Attractors of memristive parameter a. (A) Chaos-I attractor. (B) Period-I attractor. (C) Period-II attractor. (D) Chaos-II attractor.

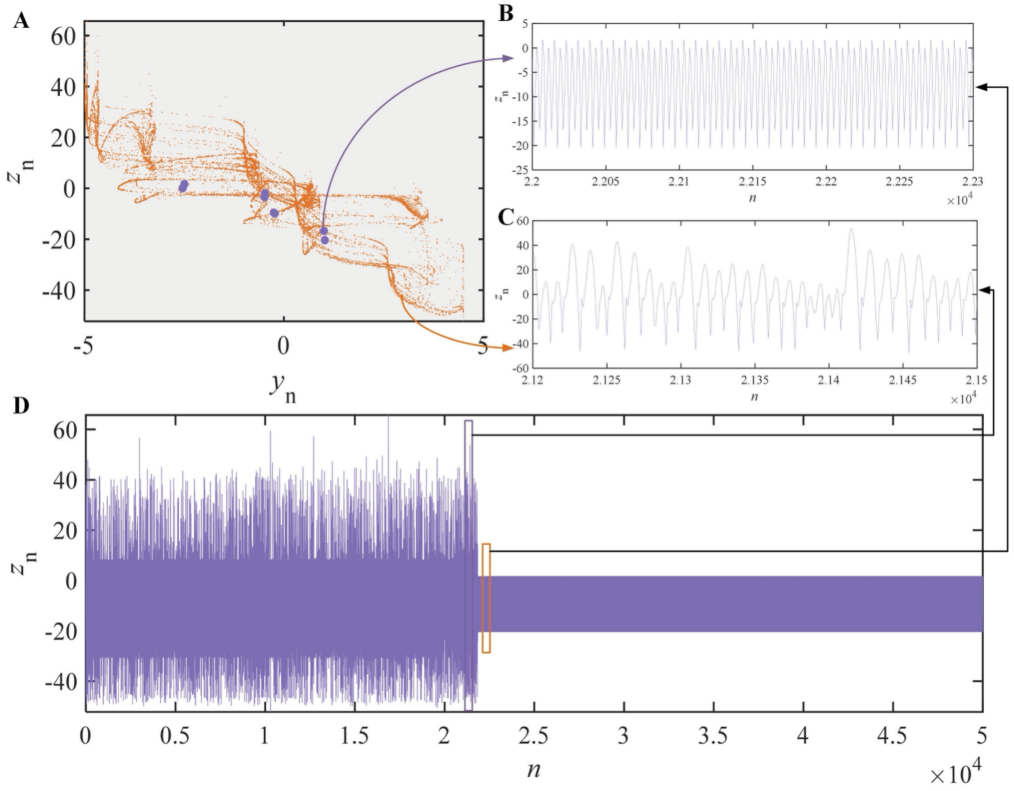

Figure 10. State transition of the system. (A) Attractor of state transition. (B) Period firing. (C) Chaos firing. (D) State-transfer firing.

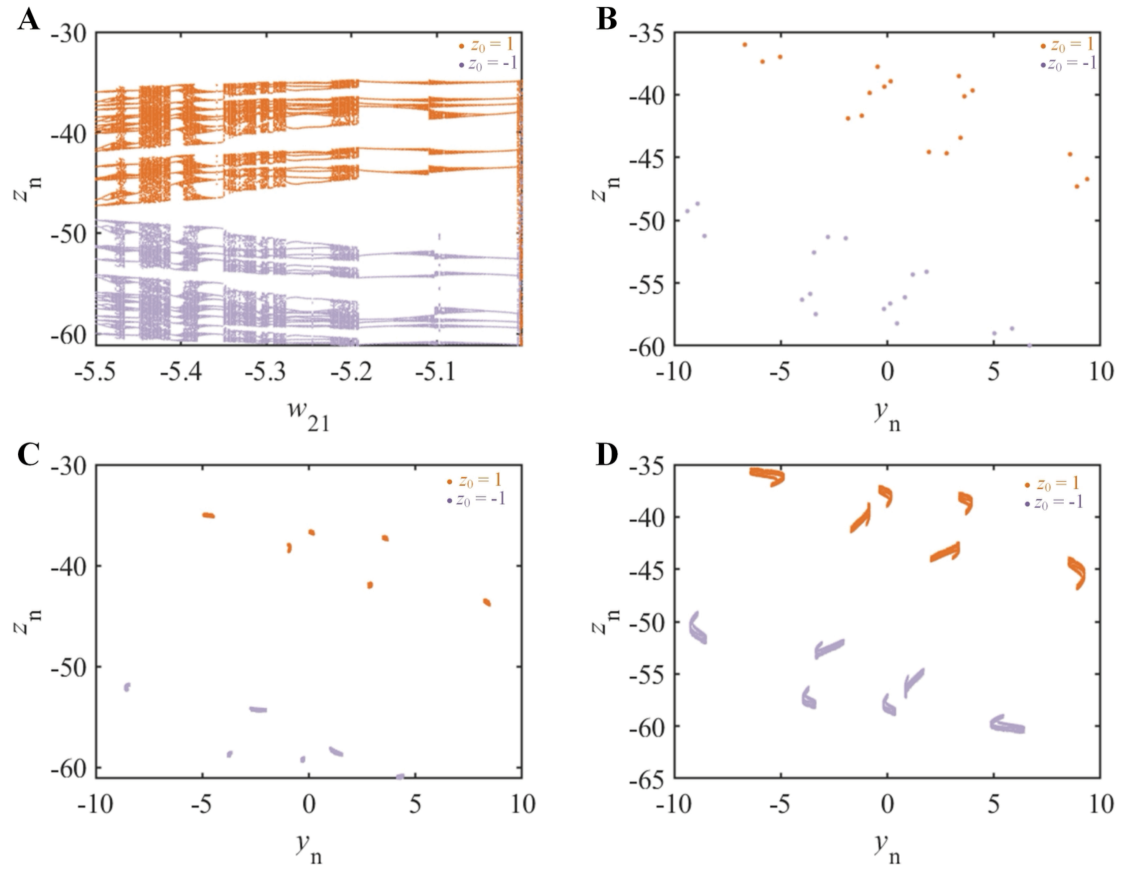

Figure 11. Multistable chaotic dynamics of the system. (A) Coexistence bifurcation diagram. (B) Coexistence period attractor, $w_{21} = -5.5$. (C) Coexistence chaos attractor-I, $w_{21} = -5.1$. (D) Coexistence chaos attractor-II, $w_{21} = -5.43$.

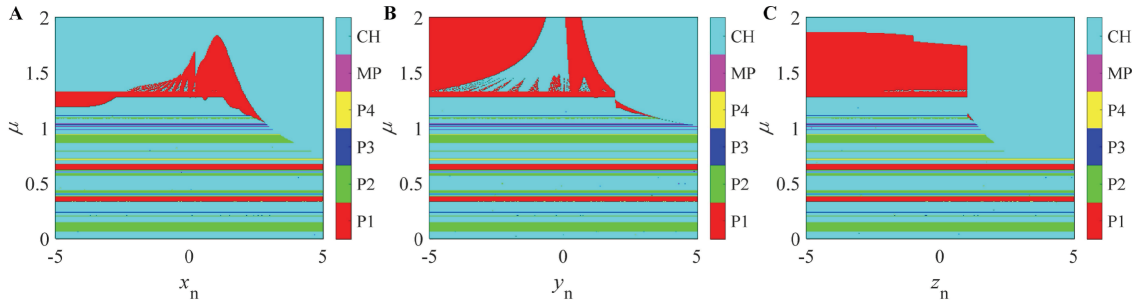

Figure 12. Attractor basin of the system. (A) x_n–μ plane. (B) y_n–μ plane. (C) z_n–μ plane. Abbreviations: CH: chaotic states; MP: Multiperiodic states.

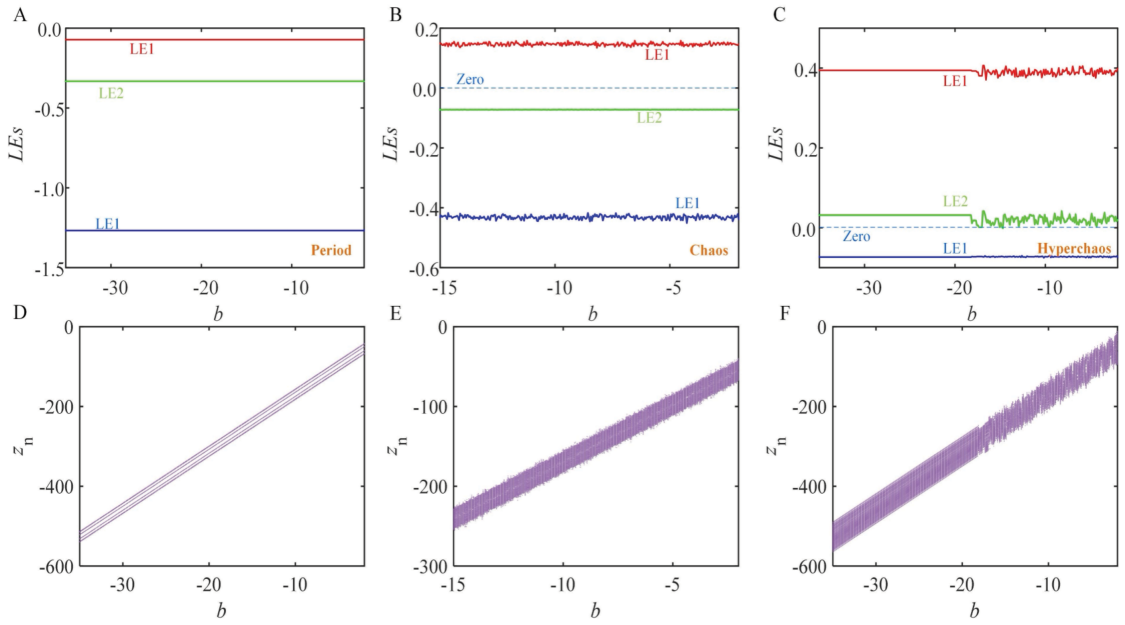

Figure 13. Offset control due to internal parameter b. (A) Bifurcation diagram and LEs, $a = 0.93$, $\mu = 0.34$, $k = 0.8$, and varying control parameters b = $(-35, -2)$. (B) LEs, $a = 0.93$, $\mu = 0.34$, $k = 1.05$, and varying control parameters $b = (-15, -2)$. (C) LEs, $a = 0.93$, $\mu = 0.34$, $k = 1.8$, and varying control parameters $b = (-35, -2)$. (D) Bifurcation diagram, $a = 0.93$, $\mu = 0.34$, $k = 0.8$, and varying control parameters $b = (-35, -2)$; (E) Bifurcation diagram, $a = 0.93$, $\mu = 0.34$, $k = 1.05$, and varying control parameters $b = (-15, -2)$. (F) Bifurcation diagram, $a = 0.93$, $\mu = 0.34$, $k = 1.8$, and varying control parameters $b = (-35, -2)$.
Abbreviation: LEs: Lyapunov exponents.

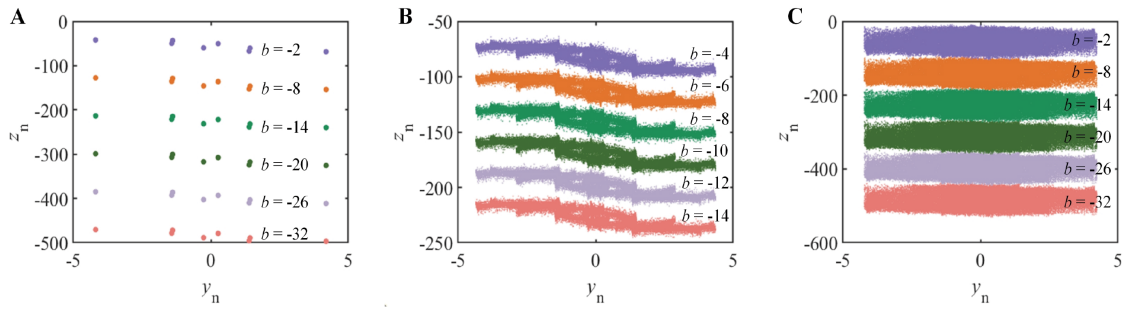

Figure 14. Attractors offset control. (A) Period attractor, $a = 0.93$, $\mu = 0.34$, $k = 0.8$. (B) Chaos attractor, $a = 0.93$, $\mu = 0.34$, $k = 0.8$. (C) Hyperchaos attractor, $a = 0.93$, $\mu = 0.34$, $k = 0.8$.

offset control method, the LEs remain nearly unchanged, ensuring that the system's state is preserved during the control process. Meanwhile, the bifurcation diagrams exhibit an overall upward trend, but their structural features remain intact, indicating that the phase trajectories of the attractors are maintained while their positions shift.

To visualize this distinctive dynamical behavior more clearly, the offset control of periodic, chaotic, and hyperchaotic attractors under modulation of the internal parameter b is illustrated in Figure 14A, 14B, and 14C, respectively. Through flexible adjustment of the internal parameters, the behavior of attractors can be effectively

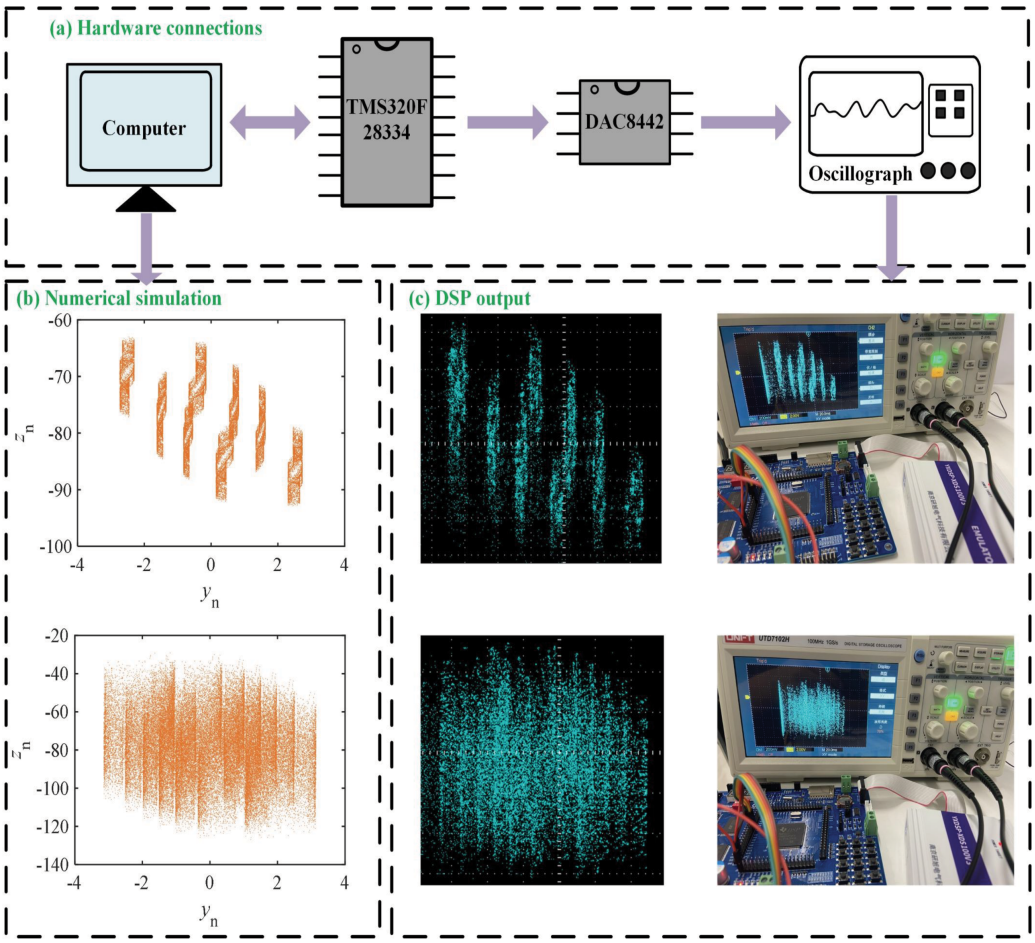

Figure 15. Hardware connections and DSP output. (A) DSP hardware connection diagram. (B) Results of Matrix Laboratory numerical simulations. (C) Attractors obtained from the digital hardware at different parameter settings.
Abbreviation: DSP: digital signal processing.

```
Initialize_System_Controller()
Disable_All_Interrupts()
function Buzz_GPIO_Init():
    Enable pull-up on GPIO54, GPIO56, GPIO57;  Configure GPIO35, GPIO36, GPIO37 as GPIO outputs;  Set initial output state high for all pins
function WriteDAC(data):
    Pull chip select low (SPISTEA = GPIO35)
    for 24 cycles (24-bit data transmission):
        Set clock high (SPICLK = GPIO36); Set data line (SPISIMO = GPIO37) based on bit value; Right shift mask for next bit; Set clock low (SPICLK)
    Pull chip select high (SPISTEA)
function adm(x, y, z, output_array):
    w11 = -3; w12 = 10;     w21 = -2; w22 = 2;       a = 0.95; b = -2;      r = 0.8; k = 1
    output_array[0] = r*x + w11*tanh(x) + w12*tanh(y) + k*tanh(z)*x
    output_array[1] = r*y + w21*tanh(x) + w22*tanh(y)
    output_array[2] = a*(sign(z+1) + sign(z-1) + z) + x + b
main():
    Initialize_System_Controller()
    Buzz_GPIO_Init()
    x[0] = 0.0, y[0] = 0.1, z[0] = 0.0;      Set GPIO35 high
    while True:
        current_state = array[3]
        adm(x[0], y[0], z[0], current_state)
        mix[0] = (current_state[1] + 4) * 7000;     # y-component          mix[1] = (current_state[2] + 140) * 460    # z-component
        x[0] = current_state[0];     # x-component          y[0] = current_state[1];     # y-component    z[0] = current_state[2]     # z-component
        dac_command_1 = 0x000000 | mix[0];     # Channel 1 data          dac_command_2 = 0x340000 | mix[1]     # Channel 2 data with different address
        WriteDAC(dac_command_1)
        WriteDAC(dac_command_2)         # Output to DAC channels
```

Figure 16. Digital signal processing code

controlled, allowing the chaotic signals generated by the model to meet industrial application requirements.

4. Digital signal processing implementation

In the engineering application of chaotic models, hardware implementation plays a crucial role. Owing to its high computational efficiency, low power consumption, and real-time processing capability, the DSP is well-suited for complex signal processing tasks. In this work, a modular design scheme was adopted, and the interconnections of the functional modules are shown in Figure 15A. The specific DSP implementation code is shown in Figure 16. The experimental setup employed the TMS320F28334 as the core DSP chip, along with a DAC8442 digital-to-analog converter to generate analog voltage sequences. These sequences were then passed through a level conversion circuit before being fed into an oscilloscope. Based on the ICs and control parameters specified in Figure 5, the program is written in the C language and preloaded into the DSP microcontroller. During operation, chaotic attractors

under different parameter settings can be obtained via the oscilloscope. Figure 15B shows the corresponding numerical simulation, while Figure 15C presents the digital hardware prototype along with the experimental attractor. The comparison between the two demonstrates strong agreement, thereby confirming the engineering feasibility of the proposed model.

5. Conclusion

This study systematically investigated the effects of EMR on neuronal dynamics by proposing a novel locally active discrete memristor model, which was incorporated into an HNN. Using nonlinear dynamical analysis, the complex behaviors of the model under different parameter conditions were revealed, including multistability and state transitions. Firstly, the mechanism underlying chaotic behavior was elucidated through equilibrium point stability analysis. Subsequently, LE spectra and bifurcation diagrams identified extensive chaotic regions and illustrated diverse attractors with different topological structures. Notably, the model exhibited an internal parameter-dependent attractor offset control mechanism, allowing flexible adjustment of attractor positions without altering their structural properties. Further implementation on a DSP platform validated the hardware feasibility of the model, demonstrating both theoretical significance and practical engineering potential. The results indicate that EMR can induce rich and complex nonlinear responses in neurons, providing new insights into the potential health impacts of long-term electromagnetic exposure. Moreover, the dynamic characteristics exhibited by the model also suggest promising applications in fields like image encryption. Future work should focus on integrating experimental data to further verify the biological relevance of the model and exploring its broader applications in medical diagnostics and information security. Ultimately, these efforts aim to deepen our understanding of electromagnetic–neural interactions and promote the development of next-generation bio-inspired artificial intelligence systems.

Acknowledgments

None.

Funding

This work was supported in part by the Liaoning Provincial Science and Technology Plan Joint Project under Grant 2024-MSLH-033, in part by Technological Innovation Projects in the Field of Artificial Intelligence in Liaoning Province under Grant 2023JH26/10300011, in part by Basic Scientific Research Projects in Department of Education of Liaoning Province under Grant LJ212410152049, in part by National Natural Science Foundation of China under Grant 62571079, Research startup fund project for introducing talents of Dalian Polytechnic University under Grant LJBKY2025070, and Doctoral Research Startup Fund Program Project of Liaoning Province under Grant 2025-BS-0471.

Conflict of interest

The authors declare that they have no competing interests.

Author contributions

Conceptualization: Fan Shi, Xianying Xu
Investigation: Fan Shi, Xiaodong Liu
Methodology: Fan Shi, Yinghong Cao
Writing–original draft: Fan Shi, Suo Gao
Writing–review & editing: Fan Shi, Jun Mou

Availability of data

Data used in this work is available from the corresponding author (xuxiany@dlpu.edu.cn) upon reasonable request.

AI Tools Statement

The authors confirm that no artificial intelligence (AI) tools were used in the preparation of this manuscript.

References

1. Bittner KC, Milstein AD, Grienberger C, Romani S, Magee JC. Behavioral time scale synaptic plasticity underlies CA1 place fields. *Science.* 2017;357(6355):1033-1036.
2. Freeman WJ. Chaos in the brain: Possible roles in biological intelligence. *Int J Intell Syst.* 1995;10(1):71-88.
3. Mahmoudvand S, Ghazavi MR, Farrokhabadi A. Nonlinear dynamic modeling and chaos analysis of aircraft landing gear under two-and three-point landings. *Nonlinear Sci Control Eng.* 2025;1(1):025280001.
4. Hopfield J. Neural networks and physical systems with emergent collective computational abilities. *Proc Natl Acad Sci U S A.* 1982;79(8):2554-2558.
5. Lin H, Wang C, Deng Q, Xu C, Deng Z, Zhou C. Review on chaotic dynamics of memristive neuron and neural network. *Nonlinear Dyn.* 2021;106(1):959-973.
6. Ma J, Tang J. A review for dynamics in neuron and neuronal network. *Nonlinear Dyn.* 2017;89(3):1569-1578.
7. Anusree M, Pramod P. Understanding chaotic neural networks: A comprehensive review. *Nonlinear Dyn.* 2025:1-16.
8. Di Ventra M, Pershin Y. On the physical properties of memristive, memcapacitive and meminductive systems. *Nanotechnology.* 2013;24(25):255201.
9. Yang F, Xu Y, Ma J. A memristive neuron and its adaptability to external electric field. *Chaos.* 2023;33(2). https://doi.org/10.1063/5.0136195
10. Xu Q, Chen X, Wu H, Iu HH, Parastesh F, Wang N. ReLU function-based locally active memristor and its application in generating spiking behaviors. *IEEE Trans Circuits Syst II Express Briefs.* 2024;71(10):4551-4555.
11. Ma T, Mou J, Chen W. Dynamics and implementation of a functional neuron model with hyperchaotic behavior under electromagnetic radiation. *Chaos Solitons Fractals.* 2025;190:115795.
12. Zhang S, Li Y, Lu D, Gao X, Li C, Chen G. A novel memristor regulation method for chaos enhancement in unidirectional ring neural networks. *IEEE Trans Circuits Syst I Regul Pap.* Published online 2025; https://doi.org/10.1109/TCSI.2025.3536028
13. Korn H, Faure P. Is there chaos in the brain? II. Experimental evidence and related models. *C R Biol.* 2003;326(9):787-840.
14. Deng Q, Wang C, Yang G, Luo D. Discrete memristive delay feedback Rulkov neuron model: Chaotic dynamics, hardware implementation and application in secure communication. *IEEE Internet Things J.* 2025;12(13):25559-25567.
15. Shi F, Cao Y, Banerjee S, Ahmad A, Mou J. A novel neural networks with memristor coupled memcapacitor-synapse neuron. *Chaos Solitons Fractals.* 2024;189:115723.
16. Liang Y, Liu K, Dong Y, Lu Z, Wang G. Capacitively coupled memristive neurons on the edge of chaos. *IEEE Trans Circuits Syst II Express Briefs.* 2024;71(8):3950-3954.

17. Zhang Z, Gao X, Cao Y, Banerjee S, Mou J. Privacy protection scheme for batch medical images based on double memristor cellular neural network. *Nonlinear Dyn.* 2025;113(9):10559-10576.
18. Lujano-Hernandez L, Munoz-Pacheco J, Sánchez-Gaspariano A. Nonlinear dynamics and experimental realization of a piecewise linear multi-scroll Hopfield neural network with a memristive synapse. *Discrete Contin Dyn Syst Ser S.* 2025:1937-1632.
https://doi.org/10.3934/dcdss.2025097
19. Gao S, Ding S, Ho-Ching Iu H, et al. A three-dimensional memristor-based hyperchaotic map for pseudorandom number generation and multi-image encryption. *Chaos.* 2025;35(7)073105.
https://doi.org/10.1063/5.0270220
20. Li F, Qin W, Xi M, Bai L, Bao B. Plane coexistence behaviors for Hopfield neural network with two-memristor-interconnected neurons. *Neural Netw.* 2025;183:107049.
21. He S, Vignesh D, Rondoni L, Banerjee S. Chaos and multi-layer attractors in asymmetric neural networks coupled with discrete fractional memristor. *Neural Netw.* 2023;167:572-587.
22. Shi F, Cao Y, Banerjee S, Mou J. A neuronal circuit based on a second-order memristor. *Nonlinear Dyn.* 2025;113(10):12165-12183.
23. Chua L. Memristors on 'edge of chaos'. *Nat Rev Electr Eng.* 2024;1(9):614-627.
24. Gao S, Iu HH-C, Erkan U, et al. A 3D memristive cubic map with dual discrete memristors: design, implementation, and application in image encryption. *IEEE Trans Circuits Syst Video Technol.* 2025;35(8):7706-7718.
25. Guo M, Yang R, Zhang M, Liu R, Zhu Y, Dou G. A novel memcapacitor and its application in a chaotic circuit. *Nonlinear Dyn.* 2021;105(1):877-886.
26. Wan Z, Pu Y-F, Lai Q. Memristive feedback-controlled chaotic system with diverse dynamics. *Nonlinear Sci Control Eng.* 2025;1(1):025310008.
27. Khan MU, Hassan B, Alazzam A, Eissa S, Mohammad B. Brain inspired iontronic fluidic memristive and memcapacitive device for self-powered electronics. *Microsyst Nanoeng.* 2025;11(1):37.
28. Mou J, Cao H, Zhou N, Cao Y. An FHN-HR neuron network coupled with a novel locally active memristor and its DSP implementation. *IEEE Trans Cybern.* 2024;54(12):7333-7342.
29. Mou J, Han Z, Cao Y, Banerjee S. Discrete second-order memristor and its application to chaotic map. *IEEE Trans Circuits Syst II Express Briefs.* 2024;71(5):2824-2828.
30. Qin M, Lai Q, Wang H, Wan Z. Complex dynamics in chain HNN with parameter-relied equilibria and memristive electromagnetic induction. *Chaos.* 2025;35(2):023123.
https://doi.org/10.1063/5.0248515
31. Min F, Ji J, Cao Y, Xu Y. Bifurcation dynamics, amplitude-frequency characteristics of Hopfield neural network and its application. *IEEE Internet Things J.* 2025;12(14):27033-27043.
https://doi.org/10.1109/JIOT.2025.3561933.
32. Gao S, Zhang Z, Li Q, et al. Encrypt a story: A video segment encryption method based on the discrete sinusoidal memristive Rulkov neuron. *IEEE Trans Depend Secure Comput.* 2025;1-15.
https://doi.org/10.1109/TDSC.2025.3603570
33. Bao H, Zhu D, Liu W, Xu Q, Chen M, Bao B. Memristor synapse-based Morris–Lecar model: Bifurcation analyses and FPGA-based validations for periodic and chaotic bursting/spiking firings. *Int J Bifurcat Chaos.* 2020;30(03):2050045.
34. Shen H, Yu F, Wang C, Sun J, Cai S. Firing mechanism based on single memristive neuron and double memristive coupled neurons. *Nonlinear Dyn.* 2022;110(4):3807-3822.
35. Mou J, Ma T, Banerjee S, Zhang Y. A novel memcapacitive-synapse neuron: Bionic modeling, complex dynamics analysis and circuit implementation. *IEEE Trans Circuits Syst I Regul Pap.* 2024;71(4):1771-1780.